

1 **Creating long term gridded fields of reference**  
2 **evapotranspiration in Alpine terrain based on a re-**  
3 **calibrated Hargreaves method**

4

5 **K. Haslinger<sup>1</sup>, A. Bartsch<sup>1</sup>**

6 [1]{Central Institute for Meteorology and Geodynamics (ZAMG), Climate Research  
7 Department, Vienna, Austria}

8 Correspondence to: K. Haslinger (klaus.haslinger@zamg.ac.at)

9

10 **Abstract**

11 A new approach for the construction of high resolution gridded fields of reference  
12 evapotranspiration for the Austrian domain on a daily time step is presented. Gridded data of  
13 minimum and maximum temperatures are used to estimate reference evapotranspiration based  
14 on the formulation of Hargreaves. The calibration constant in the Hargreaves equation is  
15 recalibrated to the Penman-Monteith equation in a monthly and station-wise assessment. This  
16 ensures on one hand eliminated biases of the Hargreaves approach compared to the  
17 formulation of Penman-Monteith and on the other hand also reduced root mean square errors  
18 and relative errors on a daily time scale. The resulting new calibration parameters are  
19 interpolated over time to a daily temporal resolution for a standard year of 365 days. The  
20 overall novelty of the approach is the use of surface elevation as the only predictor to estimate  
21 the re-calibrated Hargreaves parameter in space. A third order polynomial is fitted to the re-  
22 calibrated parameters against elevation at every station which yields a statistical model for  
23 assessing these new parameters in space by using the underlying digital elevation model of  
24 the temperature fields. With these newly calibrated parameters for every day of year and  
25 every grid point, the Hargreaves method is applied to the temperature fields, yielding  
26 reference evapotranspiration for the entire grid and time period from 1961-2013. This  
27 approach is opening opportunities to create high resolution reference evapotranspiration fields  
28 based only temperature observations, but being closest as possible to the estimates of the  
29 Penman-Monteith approach.

## 1   **1   Introduction**

2   The water balance in its most general form is determined by fluxes of precipitation, change in  
3   storage and evapotranspiration (Shelton 2009). Particularly for evapotranspiration,  
4   measurement is rather costly, since it requires sophisticated techniques like eddy correlation  
5   methods or lysimeters. In hydrology as well as agricultural sciences the actual  
6   evapotranspiration as part of the water balance equation is mostly assessed from the potential  
7   evapotranspiration (PET). PET refers to the maximum moisture loss from the surface,  
8   determined by meteorological conditions and the surface type, assuming unlimited moisture  
9   supply (Lhomme 1997). Since surface conditions determine the amount of PET, the concept  
10   of reference evapotranspiration (ET<sub>0</sub>) was introduced (Doorenbos and Pruitt, 1977). ET<sub>0</sub>  
11   refers to the evapotranspiration from a standardized vegetated surface (grass) under  
12   unrestricted water supply, making ET<sub>0</sub> independent of soil properties. Numerous methods  
13   exist for estimating ET<sub>0</sub>; differences arise in the complexity and the amount of necessary  
14   input data for calculation.

15   A standard method, recommended by the Food and Agricultural Organisation (FAO; Allen et  
16   al. 1998), is the Penman-Monteith (PM) formulation of ET<sub>0</sub>. There are of course countless  
17   other methods as thoroughly described in McMahon et al. (2013), but the PM equation is  
18   considered the most reliable estimate and serves as a standard for comparisons with other  
19   methods (Allen et al. 1998). PM is fully physically based and requires four meteorological  
20   parameters (air temperature, wind speed, relative humidity and net radiation). It utilizes  
21   energy balance calculations at the surface to derive ET<sub>0</sub> and is therefore considered a  
22   radiation based method (Xu and Singh 2000).

23   On the contrary, much simpler methods which use air temperature as a proxy for radiation  
24   (Xu and Singh 2001) are applied as alternatives for regions where the input data is not  
25   sufficient to use PM. One of these simpler methods; the method of Hargreaves (HM,  
26   Hargreaves et al. 1985), is used in this paper. It requires minimum and maximum air  
27   temperature and extra-terrestrial radiation, which can be derived from the geographical  
28   location and the day of year. Hence, HM is much broader applicable for many regions,  
29   because temperature observations are dense and easily accessible. Nevertheless, like most  
30   temperature based methods, HM has been developed for distinct studies and regions  
31   representing also distinct climate conditions (Xu and Singh, 2001). To avoid large errors,  
32   these temperature-based methods need to undergo a recalibration procedure to make them

1 applicable in different climatic regions than in those they were originally designed for  
2 (Chattopadhyay and Hulme 1997, Xu and Chen 2005).

3 In this paper, the method for constructing a dataset of ET<sub>0</sub> is presented on a daily time  
4 resolution and a 1 km spatial resolution based on the method of Hargreaves. The HM is  
5 calibrated to the PM in a station-wise assessment. Many studies describe re-calibration  
6 procedures for ET<sub>0</sub> estimations in general (Tegos et al., 2015; Oudin et al. 2005) and for the  
7 HM in particular (Pandey et al. 2014; Tabari and Talaei, 2011; Bautista et al., 2009; Gavilán  
8 et al. 2006) in order to achieve results comparable to PM. There are also some studies  
9 describing methods for creating interpolated ET<sub>0</sub> estimates (e. g. Aguila and Polo, 2011;  
10 Todorovic et al, 2013). However, two main methodological frameworks emerged for the  
11 interpolation of ET<sub>0</sub> (McVicar et al., 2007): (i) interpolation of the forcing data and then  
12 calculating ET<sub>0</sub>, or (ii) calculating ET<sub>0</sub> at every weather station followed by an interpolation  
13 of ET<sub>0</sub> onto the grid. Here we follow the first approach and combine it with methods  
14 proposed by Tegos et al. (2015) and Mancosu et al. (2014) which use spatially interpolated  
15 ET<sub>0</sub> model parameters. Gridded data of minimum and maximum temperatures are used as  
16 forcing fields for the application of the Hargreaves formulation of ET<sub>0</sub>. The novelty of this  
17 study is the application of elevation as a predictor for the interpolation of the re-calibrated  
18 HM calibration parameter. Furthermore, these new calibration parameters are also variable in  
19 time, by changing day-by-day for all days of the year. This approach goes a step further than  
20 the method of Aguilar and Polo (2011) which derived one new calibration parameter for the  
21 dry and one for the wet season of the year. An evaluation of the final gridded product is  
22 carried out by assessing different error metrics at grid points next to weather stations where  
23 PM ET<sub>0</sub> is available, and also by comparing the ET<sub>0</sub> fields with those of the operational ET<sub>0</sub>  
24 estimates based on INCA (Integrated Nowcasting through Comprehensive Analysis, Haiden  
25 et al. 2011), the nowcasting system of the Austrian weather service.

26 The presented dataset aims at using the best of two worlds by (i) using a method for  
27 estimating ET<sub>0</sub> that is calibrated to the standard algorithm as defined by the FAO and (ii)  
28 being applicable to a comprehensive, long-term forcing dataset, on a high temporal and  
29 spatial resolution.

30

## 1    **2    Forcing Data**

2    The ET<sub>0</sub> calculations are based on a high resolution gridded dataset of daily minimum and  
3    maximum temperatures calculated for the Austrian domain (SPARTACUS, see Hiebl and Frei  
4    2015), whereas the actual data stretches beyond Austria to entirely cover catchments close to  
5    the border. SPARTACUS is an operationally, daily updated dataset starting in 1961. For the  
6    ET<sub>0</sub> fields, the SPARTACUS temperature forcing is used for the period 1961-2013. The  
7    interpolation algorithm is tailored to complex, mountainous terrain with spatially complex  
8    temperature distributions. SPARTACUS also aims at ensuring temporal consistency through a  
9    fixed station network over the full time period, providing robust trend estimations in space.  
10    SPARTACUS uses the SRTM (Shuttle Radar Topography Mission, Farr and Kobrick 2000)  
11    version 2 Digital Elevation Model (DEM). The SRTM DEM is also applied in the present  
12    study.

13    SPARTACUS provides the input data for calculating ET<sub>0</sub> following the Hargreaves method  
14    (HM, Hargreaves and Samani 1982, Hargreaves and Allen 2003). However, a recalibration of  
15    HM is necessary to avoid considerable estimation errors. This is carried out in a station wise  
16    assessment. Data of 42 meteorological stations (provided by the Austrian weather service  
17    ZAMG) are used to calibrate the HM to PM on a monthly basis. Figure 1 shows the location  
18    of these stations, which are spread homogeneously over Austria and cover rather different  
19    elevations and environmental settings (Table 1). Data of daily global radiation, wind speed,  
20    humidity, maximum and minimum temperatures for the period 2004-2013 are used to  
21    calculate ET<sub>0</sub> simultaneously with HM and PM.

22

## 23    **3    Methods**

24    Numerous methods exist for the estimation of ET<sub>0</sub>, which is defined as the maximum  
25    moisture loss from a standardized, vegetated surface, determined by the meteorological  
26    forcing (Shelton, 2009). These methods can roughly be classified as temperature based and  
27    radiation based estimates (Xu and Singh, 2000, Xu and Singh, 2001, Bormann, 2011).  
28    Following the recommendations of the FAO (Allen et al. 1998) the radiation-based Penman-  
29    Monteith Method (PM) provides most realistic results and generally outperforms temperature  
30    based methods. The overall shortcoming of the PM is the data intense calculation algorithm  
31    which requires daily values of net radiation, wind speed, humidity, maximum and minimum

1 temperatures. Data coverage for these variables is usually rather sparse, particularly if gridded  
 2 data is required. ET0 following the PM is calculated as displayed in Equation 1:

$$3 \quad ET0\_p = \frac{0.408\Delta(R_N - G) + \gamma \frac{900}{T + 273} u_2 (e_s - e_a)}{\Delta + \gamma(1 + 0.34u_2)} \quad (1)$$

4 where E is the reference evapotranspiration [mm day<sup>-1</sup>], R<sub>N</sub> is the net radiation at the crop  
 5 surface [MJ m<sup>-2</sup> day<sup>-1</sup>], G is the soil heat flux density [MJ m<sup>-2</sup> day<sup>-1</sup>], T is the mean air  
 6 temperature at 2 m height [°C], u<sub>2</sub> is the wind speed at 2 m height [m s<sup>-1</sup>], e<sub>s</sub> is the saturation  
 7 vapour pressure [kPa], e<sub>a</sub> is the actual vapour pressure [kPa]; giving the vapour pressure  
 8 deficit by subtracting e<sub>a</sub> from e<sub>s</sub>; Δ is the slope of the vapour pressure curve [kPa °C<sup>-1</sup>] and γ is  
 9 the psychrometric constant [kPa °C<sup>-1</sup>]. Given the time resolution of one day the soil heat flux  
 10 term is set to zero. The calculation of the other individual terms of Equation 1 is described in  
 11 Allen et al. (1998). It should be mentioned, that the original Penman-Monteith equation  
 12 contains a “surface resistance” term, expressing the response of different vegetation types,  
 13 which is set constant for FAO PM, since it uses a standardized vegetated surface.

14 In contrast to the radiation based PM, the HM is based on daily minimum and maximum  
 15 temperatures (T<sub>min</sub>, T<sub>max</sub>). Hargreaves (1975) stated from regression analysis between  
 16 meteorological variables and measured ET0 that temperature multiplied by surface global  
 17 radiation is able to explain 94 % of the variance of ET0 for a five day period (see Hargreaves  
 18 and Allen 2003). Furthermore, wind and relative humidity explained only 10 and 9 %  
 19 respectively. Additional investigations by Hargreaves led to an assessment of surface  
 20 radiation which can be explained by extra-terrestrial radiation at the top of the atmosphere and  
 21 the diurnal temperature range as an indicator for the percentage of possible sunshine hours.  
 22 The final form of the Hargreaves equation is given by:

$$23 \quad ET0\_h = C(T_{mean} + 17.78)(T_{max} - T_{min})^{0.5} R_a \quad (2)$$

24 where ET0\_h is the reference evapotranspiration [mm day<sup>-1</sup>], T<sub>mean</sub>, T<sub>max</sub> and T<sub>min</sub> are the daily  
 25 mean, maximum and minimum air temperatures [°C] respectively and R<sub>a</sub> is the water  
 26 equivalent of the extra-terrestrial radiation at the top of the atmosphere [mm day<sup>-1</sup>]. C is the  
 27 calibration parameter of the HM and was set to 0.0023 in the original publication of  
 28 Hargreaves et al. (1985).

29 Following these formulations the ET0 for all stations is calculated for the period 2004-2013.

1 In order to achieve a meaningful representation of ET0 by HM, an adjustment of the  
2 calibration parameter ( $C_{adj}$ ) of HM is necessary, with respect to ET0 derived from PM. This is  
3 carried out on an average monthly basis for every station by the following equation, as also  
4 proposed by Bautista et al. (2009):

$$5 \quad C_{adj} = 0.0023 / (E_H / E_P) \quad (3)$$

6 where  $C_{adj}$  represents the new calibration parameter of the HM,  $E_H$  is the original ET0\_h from  
7 HM, using a C of 0.0023 and  $E_P$  is the ET0\_p from PM. As a result, a new set of C values for  
8 every month and every station is available. An analysis on the behaviour of  $C_{adj}$  in space  
9 revealed rather strong altitude dependence, particularly in the cold season. This feature  
10 enables to estimate  $C_{adj}$  in space for every grid point by using the underlying DEM of the  
11 temperature fields as a predictor.

12 As a first step, the monthly  $C_{adj}$  values at every station are linearly interpolated to daily values  
13 to avoid stepwise changes and therefore abrupt shifts of  $C_{adj}$  between months. This is carried  
14 out for a standard year with length of 365 days. The result is a time series of daily changing  
15 values of  $C_{adj}$  over the course of the year, available for every station, stretching over different  
16 altitudes and therefore yielding 42 different annual time series of  $C_{adj}$ .

17 Subsequently the daily, station-wise values of  $C_{adj}$  are interpolated in space. The analysis of  
18 the  $C_{adj}$ -altitude relationship indicated non-linear characteristics, so a third order polynomial  
19 fit was chosen. Using the underlying DEM of the SPARTACUS dataset it is possible to  
20 determine adjusted calibration parameters for every grid point in space by this relationship.  
21 The polynomial fit is applied for every day of the daily interpolated station-wise  $C_{adj}$  values,  
22 since these are changing day by day as well. The result is a gridded dataset of  $C_{adj}$  for the  
23 SPARTACUS domain for 365 time steps from January 1<sup>st</sup> to December 31<sup>st</sup>.

24 Having these gridded  $C_{adj}$  values the ET0\_h.c is calculated for every grid point and day since  
25 1961 to 2013. In the case of leap years the  $C_{adj}$  grid of February 28<sup>th</sup> is also used for February  
26 29<sup>th</sup>. The final gridded product is termed ARET (Austrian Reference EvapoTranspiration  
27 dataset) throughout the rest of the paper.

28 The ARET fields are finally evaluated against station data and another ET0 product.  
29 Unfortunately there is no long-term gridded dataset of ET0 for the Austrian domain, so we  
30 used the ET0 of the nowcasting system INCA (Integrated Nowcasting through  
31 Comprehensive Analysis, Haiden et al., 2011) which yields daily fields of ET0 based on PM

1 on 1 km grid resolution. INCA uses weather stations, remote sensing data, rainfall radar data  
2 as well as DEM information to derive nowcasting fields of several meteorological variables.  
3 INCA is operational for several years, but due to constant changes in data input quality and  
4 other improvements we chose to use only the 5-year period from 2009-2013.

5 For the skill assessment of the ARET dataset we calculate mean monthly values of mean bias,  
6 Root Mean Squared Error (RMSE) and Relative Error (RE) of those grid points in ARET as  
7 well as INCA closest to a station with PM ET<sub>0</sub>.

8

## 9 **4 Results**

10 Figure 2a shows, as an example, the daily time series of ET<sub>0</sub> as derived by PM (ET<sub>0\_p</sub>) and  
11 HM (ET<sub>0\_h</sub>) in the year 2004 at the station Grossenzersdorf. The differences between those  
12 two are obvious as ET<sub>0\_p</sub> shows clearly higher variability, with ET<sub>0\_h</sub> underestimating the  
13 upward peaks in the cold season and downward peaks in the warm season. This feature is  
14 more noticeable in Figure 2b, which shows the monthly averages over all stations, indicating  
15 the spread among all 42 stations. Here, an underestimation of the ET<sub>0\_h</sub> compared to ET<sub>0\_p</sub>  
16 from October to April is counteracted by an overestimation between May and September. On  
17 the other hand, ET<sub>0\_p</sub> shows higher spread among stations compared to ET<sub>0\_h</sub> except for  
18 November to January.

19 Figure 4 shows the adjusted C values for three exemplary stations. C<sub>adj</sub> is generally higher in  
20 winter and autumn compared to the original value indicated by the dashed line at 0.0023. It is  
21 also obvious that at station Grossenzersdorf the original value is matching rather well to the  
22 C<sub>adj</sub> from April to October, in the other months the adjusted values are clearly higher. On the  
23 contrary, at station Weissensee Gatschach C<sub>adj</sub> is lower than 0.0023 except for the months  
24 from November to February. At station Rudolfshuette-Alpinzentrum the adjusted values are  
25 above the original ones all year round, reaching the highest values in wintertime of about  
26 0.007. These results clearly underpin the necessity for a re-calibration of C in order to receive  
27 sound ET<sub>0</sub> from temperature observations.

28 For simplicity for a first assessment the monthly values of C<sub>adj</sub> were used for all days of the  
29 month, no temporal interpolation was conducted. As a result, the monthly mean bias is  
30 reduced to zero at every station. Furthermore, the RMSE has also slightly decreased by 0.1 to  
31 0.2 mm day<sup>-1</sup>, as can be seen in Figure 4a. The Relative Error (RE) has also decreased, from

1 around 45 % to fewer than 35 % in January for example (cf. Figure 4b). The improvements  
2 regarding RE in summer are lower due to the higher absolute values of ET0 in the warm  
3 season.

4 The complete monthly mean time series from 2004 to 2013 of ET0\_p, ET0\_h and ET0\_h.c  
5 for three stations are shown in Figure 5. At station Grossenzersdorf the underestimation of  
6 ET0\_h in winter is reduced as well as the overall underestimation at station Rudolfshuette-  
7 Alpinzentrum. On the other hand, the overestimation in summer at station Weissensee-  
8 Gatschach is considerably reduced with ET0\_h.c. These features in combination with the  
9 information on the altitude of the given stations provide some information on more general  
10 characteristics of  $C_{adj}$  and the effects of the calibration, which underpins an altitude-  
11 dependence of  $C_{adj}$ , which is displayed in more detail in Figure 6. It shows the monthly  
12 average  $C_{adj}$  for stations which were binned to distinct classes of altitude ranging from 100 to  
13 2300 m in steps of 100 m. As already seen in Figure 3 as an example for three stations,  $C_{adj}$  is  
14 clearly higher in winter than the unadjusted value. From April to September  $C_{adj}$  is lower than  
15 0.0023 up to altitudes of 1500 m.a.s.l., lowest values are visible in May to August between  
16 altitudes of 400 to 1000 m.a.s.l. Figure 7 displays the adjusted calibration parameters plotted  
17 against altitude for the monthly means of  $C_{adj}$ . From this Figure it comes clear that this  
18 relationship is not linear.  $C_{adj}$  is decreasing from the very low situated stations until altitudes  
19 between 500 and 1000 m.a.s.l. Going further up  $C_{adj}$  increases and one could say it might be a  
20 linear increase, particularly in winter. On the other hand, looking at the summer months the  
21 station with the highest elevation (Sonnblick, 3106 m.a.s.l.) shows somewhat lower or at least  
22 equal values of  $C_{adj}$  compared to the cluster of stations between 2000 and 2400 m.a.s.l. This  
23 feature indicates that the relationship above 1000 m.a.s.l. might not be linear. Taking all this  
24 characteristics into account, a higher order polynomial fit was chosen to describe the  $C_{adj}$ -  
25 altitude relation. .

26 The results of the spatial interpolation of  $C_{adj}$  are displayed in Figure 8, where two examples  
27 of  $C_{adj}$  distribution in space are displayed; on January 1<sup>st</sup> (a) and July 1<sup>st</sup> (b). Particularly in  
28 January the altitude dependence of the calibration parameter is clearly standing out, showing  
29 rather high values of  $C_{adj}$  in the mountainous areas. In contrast to winter the spatial variations  
30 in summer are smaller, only some central Alpine areas between 1000 and 3000 m.a.s.l. are  
31 appearing in somewhat different shading than the surrounding low lands.



1 The climatological mean (1961-2013) of the final ARET fields is displayed in Figure 9a.  
2 Lowest daily mean values of below  $1.5 \text{ mm day}^{-1}$  are apparent on the highest mountain ridges  
3 of the main Alpine crest. Highest values of  $2.4 \text{ mm day}^{-1}$  and above are found in the eastern  
4 and southern low lands. Other spatial features are visible as well, for example higher ET0 in  
5 the valleys in the far western part of Austria. This higher ET0 is driven by the longer sunshine  
6 hours in these areas, which are also known as “inner alpine dry valleys”, because rainfall  
7 approaching from the west is often screened by the mountain chains in the northwest. In the  
8 ET0 estimate this feature of less cloud cover and therefore longer sunshine durations is  
9 reflected in the higher Diurnal Temperature Range (DTR), yielding larger values in that  
10 particular area. A similar characteristic is apparent in the very south of Austria. Here ET0 is  
11 higher as well, compared to topographically similar regions on the northern rim of the Alps.  
12 This is also connected to the longer sunshine hours which enhance indirectly ET0 through  
13 higher DTR values.

14 Figure 9b shows the ET0 field of August 8<sup>th</sup> 2013. For the first time on that particular day,  
15 temperatures reached above  $40 \text{ }^\circ\text{C}$  in Austria at some stations in the east and south. Values of  
16 ET0 are particularly high, reaching up to  $7 \text{ mm day}^{-1}$  in some areas in the southeast. That day  
17 was also characterized by an approaching cold front, which brought rain, dropping  
18 temperatures and overcast conditions from the west. These conditions were featured as well in  
19 the ET0 field, showing a considerable gradient from west to east, with almost zero ET0 at the  
20 headwaters of the Inn River in the far southwest of the domain. Furthermore, the implications  
21 of overcast conditions in the west with lower altitudinal gradients of ET0 compared to the east  
22 with sunny conditions and distinct gradients along elevation are visible.

23 July, the month with the highest absolute values of ET0 shows considerable variations in the  
24 last 53 years. As an example, the mean anomaly of ET0 in July of 1983 with respect to the  
25 July mean of 1961-2013 is displayed in Figure 10a. This month was characterized by a  
26 considerable heat wave and mean temperature anomalies of  $+3.5 \text{ }^\circ\text{C}$  which also affected ET0.  
27 The absolute anomaly of ET0 reaches above  $1 \text{ mm day}^{-1}$  with respect to the climatological  
28 mean in some areas. The relative anomaly is in a range between 10 to 30 % (Figure 10c). July  
29 of 1979 was rather cool instead with temperatures  $1.5 \text{ }^\circ\text{C}$  below the climatological mean and  
30 accompanied by a strong negative anomaly in sunshine duration, particularly in the areas  
31 north of the main Alpine crest. These characteristics implicated a distinctly negative anomaly  
32 of ET0 in this particular month (Figure 10b). The absolute anomaly stretches between 0 and

1 more than  $-1 \text{ mm day}^{-1}$ , which is equivalent to a relative anomaly of 0 to -30 % (Figure 10d).  
2 The negative signal is stronger in the areas north of the Alpine crest, zero anomalies are found  
3 in some areas in the south.

4 In Figure 11 the overall benefits of the re-calibration of the HM are revealed. It shows the  
5 mean ET0 in July 2012, a month accompanied by a considerable heat wave at the beginning  
6 and an overall temperature anomaly of around  $+2 \text{ }^{\circ}\text{C}$ . In Figure 11b the ET0 field of the  
7 original HM formulation without calibration is shown, and Figure 11a displays the results  
8 with re-calibration as described in this study. Overall, the gradient along elevation of ET0 is  
9 larger in the non-calibrated field. Particularly in this time of the year with large absolute  
10 values, the re-calibration has a considerable impact, although  $C_{\text{adj}}$  in July is relatively small  
11 compared to winter. As shown before (cf. Figure 3), the ET0 estimation using the original C  
12 is good for July in the very lowlands, since biases tend to be rather small. However, going to  
13 higher elevations, the overestimation of the original HM is rather pronounced. Mean biases  
14 reach  $+1 \text{ mm day}^{-1}$  or +30 % over large parts of the domain. This signal switches to negative  
15 biases of  $-0.5 \text{ mm day}^{-1}$  (-25 %) above 1500 m.a.s.l.

16 The overall performance of ARET compared to the station wise PM estimates is displayed in  
17 Figure 12. 12a shows the monthly bias of the original HM ET0 and the calibrated ET0 of the  
18 nearest grid point. The bias is clearly reduced in nearly all months. However, in April, as the  
19 only exception, the bias of the calibrated grid point values is larger than the bias of the  
20 original estimation. The biases concerning different levels of altitude are reduced as well, as  
21 can be seen in Figure 12b which shows the biases in July and Figure 12c displaying the biases  
22 in January.

23 A comparison between ARET and INCA ET0 and station based PM ET0 is given in Figure  
24 13, showing ET0 on two different days in summer 2013. The first example (Figures 13a and  
25 13b) is June the 4<sup>th</sup> 2013, a day with mostly overcast conditions, lower than average  
26 temperatures of between 7 to 12  $^{\circ}\text{C}$  and high relative humidity, it was the time after a big  
27 flood event in northern Austria. ARET is clearly overestimating ET0 by a median difference  
28 of  $+1 \text{ mm day}^{-1}$  across all stations as shown by the boxplot in Figure 13c. INCA has a median  
29 difference of nearly zero, although the spread is larger than in ARET. Another example is  
30 July 23<sup>rd</sup> 2013 (Figure 13d and 13e) which characterized by temperatures ranging between 20  
31  $^{\circ}\text{C}$  in the West and 29  $^{\circ}\text{C}$  in the east, accompanied by some rainfall in the West and South.  
32 ET0 in both ARET and INCA range between 3 and 6  $\text{mm day}^{-1}$ , although INCA shows a

1 general overestimation with a median difference around  $+0.5 \text{ mm day}^{-1}$  (Figure 13f). On the  
2 other hand median differences of ARET compared to stations are around zero.  
3 However, comparing error characteristics in ARET and INCA against station data (Table 2)  
4 for the period 2009-2013 reveals only minor differences. The mean bias all year round is  
5 lower in INCA ( $0.03 \text{ mm day}^{-1}$ ) compared to ARET ( $0.12 \text{ mm day}^{-1}$ ). Considering monthly  
6 mean values the spread is rather similar spanning  $-0.30$  to  $0.66 \text{ mm day}^{-1}$  in INCA and  $-0.17$   
7 to  $0.80 \text{ mm day}^{-1}$  in ARET. The highest monthly mean values are in both dataset found in  
8 April (ARET:  $0.80 \text{ mm day}^{-1}$ , INCA:  $0.66 \text{ mm day}^{-1}$ ) and May (ARET:  $0.79 \text{ mm day}^{-1}$ , INCA:  
9  $0.51 \text{ mm day}^{-1}$ ). The RMSE is slightly lower in ARET reaching maximum values in June of  
10  $1.42 \text{ mm day}^{-1}$  compared to INCA with  $1.80 \text{ mm day}^{-1}$ . The overall mean RMSE is  $0.89 \text{ mm}$   
11  $\text{day}^{-1}$  in ARET and  $1.05 \text{ mm day}^{-1}$  in INCA. Concerning the RE the characteristics are similar  
12 to the bias and the RMSE, with only minor differences between ARET and INCA. The RE in  
13 ARET ranges between  $+35 \%$  (April) and  $-15 \%$  (November) and in INCA these are rather  
14 similar spanning  $+25 \%$  (February) and  $-18 \%$  (November).

15

## 16 **5 Discussion**

17 By comparing the characteristics of  $ET_0$  based on HM and PM on a daily time step it came  
18 clear that a re-calibration of  $C$  within the formulation of Hargreaves follows distinct patterns.  
19 The values of  $C_{adj}$  show markedly variations in space and time (over the course of the year). It  
20 turned out, that a monthly re-calibration of  $C$  reveals an annual cycle of  $C_{adj}$ , with  $C_{adj}$  being  
21 close to the original value of  $0.0023$  in the warm season (April-October) and low elevations.  
22 Going to higher elevations,  $C_{adj}$  decreases until roughly  $1000 \text{ m.a.s.l.}$  Reaching altitudes  
23 above  $1700 \text{ m.a.s.l.}$ ,  $C_{adj}$  has generally a higher value than Hargreaves' original value,  
24 particularly during the cold season (November-March). This altitude dependency of the  
25 calibration parameter in HM is mentioned in Samani (2000), but the authors also claimed that  
26 this relationship may be affected by different latitudes. Aguila and Polo (2011) also found that  
27 the original HM using a  $C$  of  $0.0023$  underestimates  $ET_0$  at higher elevations and defined a  
28 value of  $0.0038$  at an elevation of  $2500 \text{ m.a.s.l.}$  However, this altitude dependency of  $C$  turned  
29 out to be more complex, as we are able to display, showing a distinct variation throughout the  
30 year along with elevation.

31 To reveal the sources of this altitude dependence of  $C$  some additional analysis was done. In  
32 general, the HM utilizes the Diurnal Temperature Range (DTR,  $T_{max}$  minus  $T_{min}$ ) to mimic the

1 amount of global radiation at the land surface. Clear sky conditions are usually associated  
2 with higher DTR. There is more heating during daytime due to large proportions of direct  
3 solar radiation, whereas at night time temperatures drop further down since the outgoing long-  
4 wave radiation is not reflected by clouds. Numerous studies investigating the relationship  
5 between DTR and radiation (Pan et al., 2013; Makowski et al., 2009; Bindi and Miglietta,  
6 1991; Bristow and Campbell, 1984) , which show considerable correlations. For example  
7 Makowski et al. 2009 reported a correlation coefficient of 0.87 of the annual means of DTR  
8 and solar radiation averaged over 31 stations across Europe.

9 Figure 14 shows the linear regression coefficients of the square root of DTR and Global Top-  
10 Of-Atmosphere (TOA) radiation ratio on a daily time scale at the 42 stations used in this  
11 study. The idea is to get a better understanding of the parameterization embedded in HM,  
12 which tries to assess the amount of global radiation via the DTR and the TOA radiation. The  
13 coefficients show a distinct altitudinal dependency, particularly in winter. In January the  
14 coefficients are generally high at altitudes between 300 and 1100 m.a.s.l. At higher elevations  
15 they are dropping considerably, getting slightly negative above 3000 m.a.s.l. at station  
16 Sonnblick. This altitude dependency is also apparent in the transitional season (c.f. Figure 14;  
17 April and October) although not as pronounced as in winter. In July the coefficients are  
18 generally higher, roughly ranging between 0.15 and 0.30, with no change along altitude.

19 The reasons for the patterns in Figure 14 seem to be rooted in the lower atmospheric mixing  
20 ratios at the lowest stations, some of them located in, or nearby cities, which might dampen  
21 the DTR, although clear sky conditions are apparent. At moderate altitudes between 400 and  
22 1500 m.a.s.l. the daily temperature amplitude is more dominantly driven by surface energy  
23 balance processes which reflects higher regression coefficients. Going further up, the  
24 proportion of the DTR which is determined by large scale air mass changes rises, as the  
25 station locations reach up above the planetary boundary layer into the free atmosphere. So for  
26 any given value of cloudiness, DTR is much smaller in winter and high elevations than in low  
27 elevation environments where boundary layer processes are dominant. This means for  
28 yielding realistic values of global radiation relative to TOA radiation, a much higher  $C_{adj}$   
29 value is needed to compensate for this.

30 Although these circumstances seem to be a drawback of the methodology, the overall effect is  
31 only minor. Figure 15 shows the HM ET0 in dependence of the DTR and the daily mean  
32 temperature. At low daily mean temperatures, between -10 and +10 °C, the contour lines

1 determining the value of ET<sub>0</sub> are rather steep. This implies that a change in DTR has only  
2 minor effects on the ET<sub>0</sub> outcome, whereas a change in daily mean temperature is more  
3 important.

4 However, the procedure of altering the coefficient C has also implications on the variability of  
5 ET<sub>0</sub> on a daily time scale. As was visible in Figure 2a the variability of ET<sub>0</sub> based on HM is  
6 lower than using PM. The presented re-calibration has only little effect on the enhancement of  
7 variability. By scaling C, variability is slightly enhanced in those areas and time of the year  
8 where C<sub>adj</sub> is higher than 0.0023. This is the case for most of the time and widespread areas,  
9 but there are regions or altitudinal levels where the opposite is taking place. As is visible in  
10 Figure 6 areas up to 1500 m.a.s.l. show lower than original values of C<sub>adj</sub> in the summer  
11 months. There are particular areas in June between altitudes of 500 to 1000 m.a.s.l. that show  
12 the largest deviation from the original value. In these areas variability is lower in the re-  
13 calibrated version. On the other hand the benefit of an ET<sub>0</sub> formulation being unbiased  
14 compared to the reference of PM may overcome these shortcomings.

15 Evaluating both the ARET and INCA gridded ET<sub>0</sub> estimates against station based ET<sub>0</sub>  
16 revealed only minor differences in Bias, RMSE and RE, which underpins the strength of the  
17 proposed calibration method. However, there are situations where the deviations compared to  
18 station based ET<sub>0</sub> are particularly large in both the ARET and the INCA dataset. As an  
19 example for overcast conditions after a considerable amount of rainfall for a couple of days  
20 we compared ARET to INCA ET<sub>0</sub> (cf. Figure 13) and found that ARET clearly overestimates  
21 ET<sub>0</sub>. Under the given circumstances ARET cannot compete with INCA, which considers,  
22 through using PM, information on relative humidity, which might has a strong forcing on ET<sub>0</sub>  
23 on that particular day, information that is not available in the ARET estimate. On the other  
24 hand on a typical sunny summer day INCA overestimates ET<sub>0</sub>, where ARET is rather close to  
25 the station estimates. There might be some biases in the radiation analysis in INCA causing  
26 this deviation from the station data. Global Radiation is calculated based on sunshine duration  
27 estimates (blended remote sensing and station data) driving a simple radiation model (Haiden  
28 et al. 2011).

29 As shown in the evaluation of the ARET fields against INCA the error characteristics are  
30 rather similar, although in INCA ET<sub>0</sub> is calculated using PM. The calibration of HM, though  
31 very simple, yields very satisfying results of the final product. Particularly when considering  
32 Austrian topography it comes clear that using a method like HM without calibration has major

1 impacts on the result. Using non-calibrated HM ET0 data for rainfall-runoff modelling for  
2 example would introduce large errors and uncertainties. Given the fact that gridded data of  
3 ET0 based on PM are only available for a rather short time period from the INCA system, the  
4 ARET dataset provides a sound alternative for ET0 estimates on a high spatial resolution  
5 covering the last 53 years.

6

## 7 **6 Conclusion**

8 In this paper a gridded dataset of ET0 for the Austrian domain from 1961-2013 on daily time  
9 step is presented. The forcing fields for estimating ET0 are daily minimum and maximum  
10 temperatures from the SPARTACUS dataset (Hiebl and Frei 2015). These fields are used to  
11 calculate ET0 by the formulation of Hargreaves et al. (1985). The HM is calibrated to the  
12 Penman-Monteith equation, which is the recommended method by the FAO (Allen et al.  
13 1998). This is done using a set of 42 meteorological stations from 2004-2013, which have full  
14 data availability for calculating ET0 by PM. The adjusted monthly calibration parameters  $C_{adj}$   
15 are interpolated in time (resulting in daily  $C_{adj}$  for a standard year) and space (resulting in  $C_{adj}$   
16 for every grid point of SPARTACUS and day of year). With these gridded  $C_{adj}$  the daily fields  
17 of reference evapotranspiration are calculated for the time period from 1961-2013.

18 This dataset is highly valuable for users in the field of hydrology, agriculture, ecology etc. as  
19 it provides ET0 in a high spatial resolution and a long time period. Data for calculating ET0  
20 by recommended PM is usually not available for such long time spans and/or with this spatial  
21 and temporal resolution. However, the method presented in this study combined both  
22 strengths of long time series, high spatial and temporal resolution provided by the temperature  
23 based HM and the physical more realistic radiation based PM by adjusting HM.

24

25

## 26 **Acknowledgements**

27 The authors want to thank the Federal Ministry of Science, Research and Economy (Grant  
28 1410K214014B) for financial support. We also like to thank Johann Hiebl for providing the  
29 SPARTACUS data and for fruitful discussions on the manuscript. The Austrian Weather  
30 Service (ZAMG) is acknowledged for providing the data of 42 meteorological stations. We

1 would also like to thank two anonymous reviewers for the valuable comments which  
2 improved the manuscript substantially.  
3

## 1 **References**

- 2 Aguila, C., and Polo, M. J.: Generating reference evapotranspiration surfaces from the  
3 Hargreaves equation at watershed scale, *Hydrol. Earth Syst. Sci.*, 15, 2495–2508, 2011.
- 4 Allen, R. G., Pereira, L. S., Raes, D., and Smith, M.: Crop evapotranspiration – Guidelines for  
5 computing crop water requirements, FAO Irrigation and drainage paper 56, Rome, 15 pp,  
6 1998.
- 7 Bautista, F., Bautista, D., and Delgado-Carranza, C.: Calibrating the equations of Hargreaves  
8 and Thornthwaite to estimate the potential evapotranspiration in semi-arid and subhumid  
9 tropical climates for regional applications, *Atmósfera* 22(4), 331-348, 2009.
- 10 Bindi, M., and Miglietta, F.: Estimating daily global radiation from air temperature and  
11 rainfall measurements, *Clim. Change*, 1, 117-124, 1991.
- 12 Bormann, H.: Sensitivity analysis of 18 different potential evapotranspiration models to  
13 observed climatic change at German climate stations, *Clim. Ch.*, 104, 729-753, 2011.
- 14 Bristow, K. L., and Campbell, G. S.: On the relationship between incoming solar radiation  
15 and daily maximum and minimum temperature, *Agric. Forest. Meteorol.*, 31(2), 159-166,  
16 1984. Chattopadhyay N. and Hulme M.: Evaporation and potential evapotranspiration in India  
17 under conditions of recent and future climate changes, *Agric. Forest. Meteorol.* 87, 55-74,  
18 1997.
- 19 Doorenbros, J., and Pruitt, O. W.: Crop water requirements. FAO Irrigation and Drainage  
20 Paper 24, Rome, 144 pp, 1977.
- 21 Farr, T.G., Kobrick, M.: Shuttle Radar Topography Mission produces a wealth of data, *Amer.*  
22 *Geophys. Union Eos*, 81, 583-585, 2000.
- 23 Gavilán, P., Lorite, I. J., Tornero, S., and Berengena, J.: Regional calibration of Hargreaves  
24 equation for estimating reference ET in a semiarid environment, *Agr. Water Manage.*, 81,  
25 257-281, 2006.
- 26 Haiden, T., Kann, A., Wittmann, C., Pistotnik, G., Bica, B. and Gruber C.: The Integrated  
27 Nowcasting through Comprehensive Analysis (INCA) System and Its Validation over the  
28 Eastern Alpine Region, *Weather Forecast.*, 26, 166-183, 2011.



- 1 Hargreaves, G. H., and Allen, R.: History and Evaluation of Hargreaves Evapotranspiration  
2 Equation, *J. Irrig. Drain Eng.*, 129(1), 53-63, 2003.
- 3 Hargreaves, G. H., and Samani, Z. A.: Estimating potential evapotranspiration, *J. Irrig. Drain*  
4 *Eng.*, 108(3), 225-230, 1982.
- 5 Hargreaves, G. H., and Samani, Z. A.: Reference crop evapotranspiration from temperature,  
6 *Appl. Eng. Agric.*, 1, 96-99, 1985.
- 7 Hargreaves, G. H.: Moisture Availability and Crop Production, *Trans. ASABE*, 18 (5): 980-  
8 984, 1975.
- 9 Hargreaves, G. L., Hargreaves, G. H., and Riley, J. P.: Irrigation water requirements for  
10 Senegal River Basin, *J. Irrig. Drain. Eng.*, 111(3), 265-275, 1985.
- 11 Hiebl, J., and Frei, C.: Daily temperature grids for Austria since 1961 – concept, creation and  
12 applicability, submitted to *Theor. Appl. Climatol.*
- 13 Lhomme, J.-P.: Towards a rational definition of potential evapotranspiration, *Hydrol. Earth*  
14 *Sys. Sci.*, 1(2), 257-264, 1997.
- 15 Mancosu, N., Snyder, R. L., and Spano, D.: Procedures to Develop a Standardized Reference  
16 Evapotranspiration Zone Map, *J. Irrig. Drain Eng.*, 140, A4014004, 2014.
- 17 Makowski, K., Jaeger E. B., Chiacchio, M., Wild, M., Ewen, T., and Ohmura, A.: On the  
18 relationship between diurnal temperature range and surface solar radiation in Europe, *J.*  
19 *Geophys. Res.*, 114, D00D07, 2009.
- 20 McMahon, T. A., Peel, M. C., Lowe, L., Srikanthan, R., and McVicar, T. R.: Estimating  
21 actual, potential, reference crop and pan evaporation using standard meteorological data: a  
22 pragmatic synthesis, *Hydrol. Earth Sys. Sci.*, 17, 1331–1363, 2013.
- 23 McVicar, T. R., Van Niel, T. G., Li, L., Hutchinson, M. F., Mu, X.-M., and Liu, Z.-H.:  
24 Spatially distributing monthly reference evapotranspiration and pan evaporation considering  
25 topographic influences, *J. Hyd.*, 338, 196-220, 2007.
- 26 Pan, T., Wu, S., Dai, E., and Liu, Y.: Estimating the daily global solar radiation spatial  
27 distribution from diurnal temperature ranges over the Tibetan Plateau in China, *Ap. Energy*,  
28 107, 384-393, 2013.

- 1 Pandey, V., Pandey, P. K., and Mahanta, A. P.: Calibration and performance verification of  
2 Hargreaves Samani equation in a humid region, *Irrig. and Drain.*, 63, 659–667, 2014.
- 3 Samani, Z.: Estimating Solar Radiation and Evapotranspiration Using Minimum  
4 Climatological Data (Hargreaves-Samani equation), *J. Irr. Drain. Eng.*, 126 (4), 265-267,  
5 2000.
- 6 Shelton, M. L.: *Hydroclimatology*, Cambridge University Press, Cambridge, United  
7 Kingdom, 2009.
- 8 Tabari, H. and Talaei, P.: Local Calibration of the Hargreaves and Priestley-Taylor Equations  
9 for Estimating Reference Evapotranspiration in Arid and Cold Climates of Iran Based on the  
10 Penman-Monteith Model, *J. Hydrol. Eng.*, 16(10), 837-845, 2011.
- 11 Tegos, A., Malamos, M., and Koutsoyiannis, D.: A parsimonious regional parametric  
12 evapotranspiration model based on a simplification of the Penman–Monteith formula, *J. Hyd.*,  
13 524, 708-714, 2015.
- 14 Todorovic, M., Karic, B., and Pereira, L. S.: Reference evapotranspiration estimate with  
15 limited weather data across a range of Mediterranean climates, *J. Hyd.*, 481, 166-176, 2011.
- 16 Xu, C.-Y., and Chen D.: Comparison of seven models for estimation of evapotranspiration  
17 and groundwater recharge using lysimeter measurement data in Germany, *Hydrol. Processes*,  
18 19, 3717-3734, 2005.
- 19 Xu, C.-Y., and Singh, V. P.: Evaluation and generalization of radiation-based equations for  
20 calculating evaporation, *Hydrol. Processes*, 14, 339-349, 2000.
- 21 Xu, C.-Y., and Singh, V. P.: Evaluation and generalization of temperature-based equations for  
22 calculating evaporation, *Hydrol. Processes*, 14, 339-349, 2001.
- 23

1 Table 1. Location, altitude and setting of the 42 meteorological stations used for calibration.

	Station	Lon (°)	Lat (°)	Alt (m)	Setting
1	Aflenz	15.24	47.55	783	Mountainous
2	Alberschwende	9.85	47.46	715	Mountainous
3	Arriach	13.85	46.73	870	Mountainous
4	Bregenz	9.75	47.50	424	Lakeside
5	Dornbirn	9.73	47.43	407	Valley
6	Feldkirchen	14.10	46.72	546	Valley
7	Feuerkogel	13.72	47.82	1618	Summit
8	Fischbach	15.64	47.44	1034	Mountainous
9	Galzig	10.23	47.13	2084	Alpine
10	Graz Universitaet	15.45	47.08	366	City
11	Grossenzersdorf	16.56	48.20	154	Lowland
12	Gumpoldskirchen	16.28	48.04	219	Lowland
13	Irdning Gumpenstein	14.10	47.50	702	Valley
14	Ischgl Idalpe	10.32	46.98	2323	Alpine
15	Jenbach	11.76	47.39	530	Valley
16	Kanzelhoehe	13.90	46.68	1520	Summit
17	Krems	15.62	48.42	203	Lowland
18	Kremsmünster	14.13	48.06	382	Lowland
19	Langenlois	15.70	48.47	207	Lowland
20	Lilienfeld Tarschberg	15.59	48.03	696	Mountainous
21	Lofereralm	12.65	47.60	1624	Alpine
22	Lunz am See	15.07	47.85	612	Valley
23	Lutzmannsburg	16.65	47.47	201	Lowland

24	Mariapfarr	13.75	47.15	1153	Mountainous
25	Mariazell	15.30	47.79	864	Mountainous
26	Neumarkt	14.42	47.07	869	Mountainous
27	Patscherkofel	11.46	47.21	2247	Summit
28	Poertschach	14.17	46.63	450	Lakeside
29	Retz	15.94	48.76	320	Lowland
30	Reutte	10.72	47.49	842	Valley
31	Rudolfshuette-Alpinzentrum	12.63	47.13	2304	Alpine
32	Schaerding	13.43	48.46	307	Lowland
33	Schmittenhoehe	12.74	47.33	1973	Alpine
34	Sonnblick	15.96	47.05	3109	Summit
35	Spittal Drau	13.49	46.79	542	Valley
36	Villacheralpe	13.68	46.60	2156	Summit
37	Virgen	12.46	47.00	1212	Valley
38	Weissensee Gatschach	13.29	46.72	945	Lakeside
39	Wien Donaufeld	16.43	48.26	161	City
40	Wien Hohewarte	16.36	48.25	198	City
41	Wien Unterlaa	16.42	48.12	201	City
42	Wolfsegg	13.67	48.11	638	Lowland

---

1

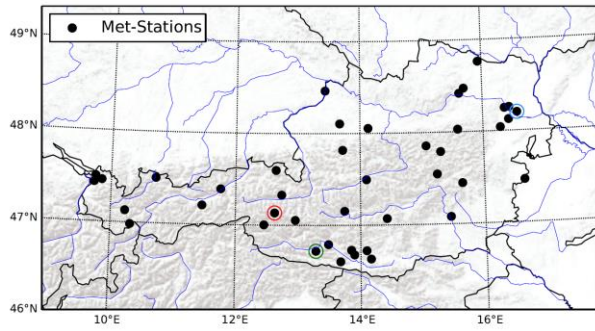
2

1 Table 2. Error Characteristics of ARET and INCA against station data

	Bias [mm/d]		RMSE [mm/d]		RE [%]	
	ARET	INCA	ARET	INCA	ARET	INCA
January	-0.01	-0.05	0.29	0.34	1	-7
February	-0.17	-0.30	0.60	0.65	-12	-25
March	0.04	-0.23	0.84	0.89	4	-14
April	0.80	0.66	1.34	1.59	35	28
May	0.79	0.51	1.38	1.58	29	19
June	0.19	-0.24	1.42	1.80	6	-8
July	0.39	0.31	1.29	1.58	12	9
August	-0.09	-0.01	1.16	1.42	-1	1
September	-0.14	-0.10	0.96	1.11	-6	-4
October	-0.15	-0.06	0.57	0.69	-8	-3
November	-0.03	0.01	0.43	0.54	2	5
December	-0.16	-0.18	0.39	0.43	-15	-18
Year	0.12	0.03	0.89	1.05	4	-1

2

1

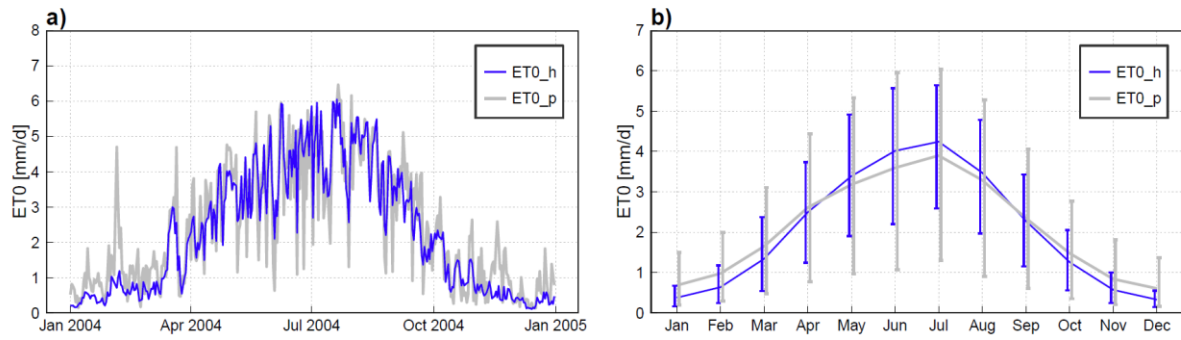


2

3

4 Figure 1. Location of the meteorological stations used for calibration; coloured circles around  
5 points indicate stations that are exemplary displayed in other plots: Grossenzersdorf (blue),  
6 Weissensee Gatschach (green) and Rudolfshuette-Alpinzentrum (red).

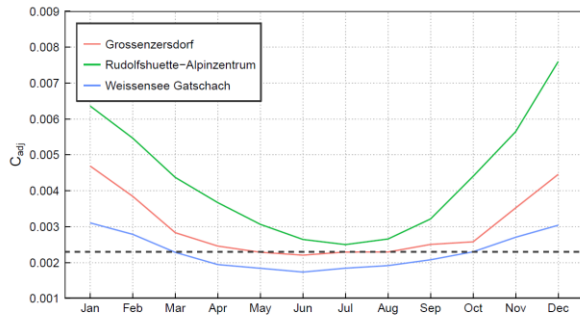
7



1  
2  
3  
4  
5  
6

Figure 2. Daily time series of ET0 in 2004 for ET0 based on PM (ET0\_p) and HM (ET0\_h) at the station Grossenzersdorf (a); Monthly mean ET0 from 2004 to 2013 averaged over all stations, error bars denote the spread among all stations (b).

1



2

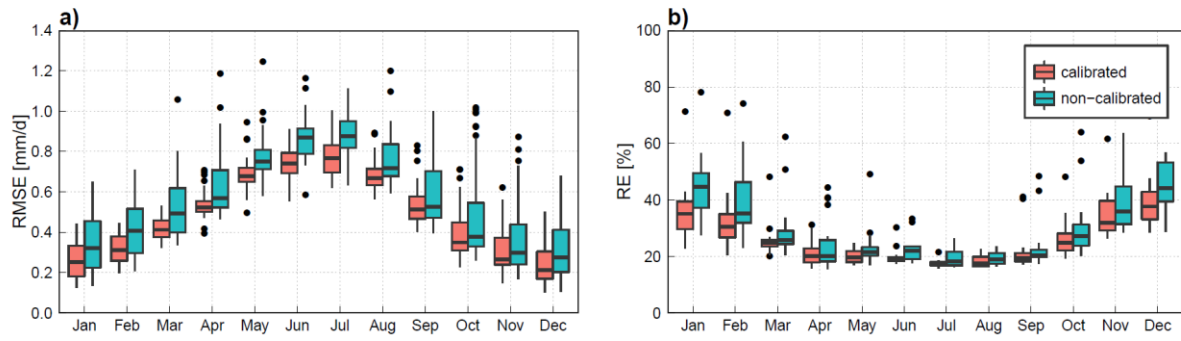
3

4 Figure 3. Monthly values of  $C_{adj}$  at three different stations, the dashed black lines indicates the  
5 original C value of 0.0023 from Hargreaves et al. (1985).

6



1

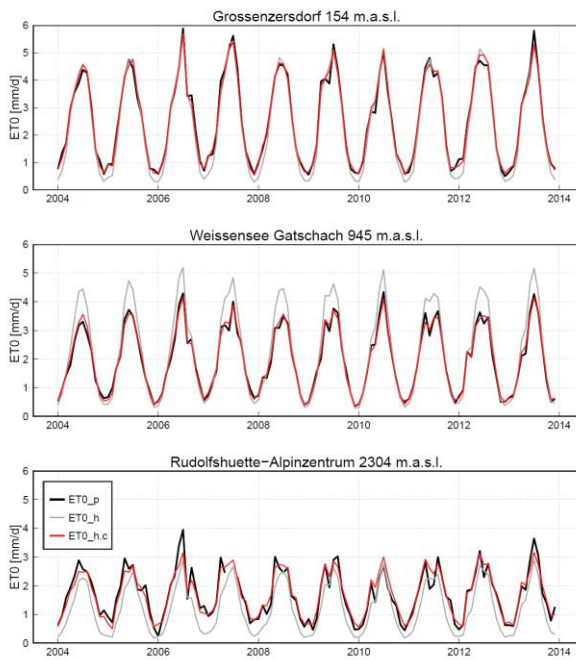


2

3

4 Figure 4. Monthly Root Mean Square Error (a) and monthly Relative Error (b) between daily  
5 ET0\_p and ET0\_h (black) and ET0\_p and ET0\_h.c (red).

1



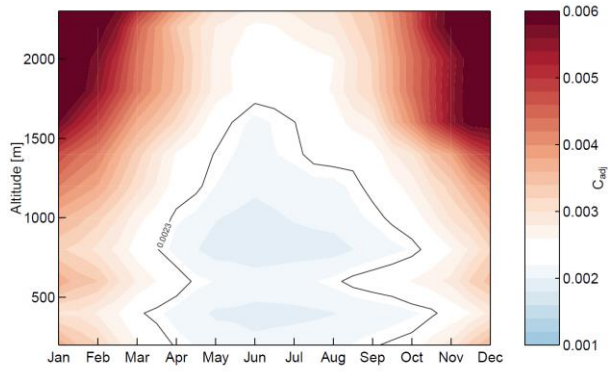
2

3

4 Figure 5. Monthly ET0 sums derived from ET0\_p, ET0\_h and ET0\_h.c for three stations  
5 located at different altitudes.

6

1

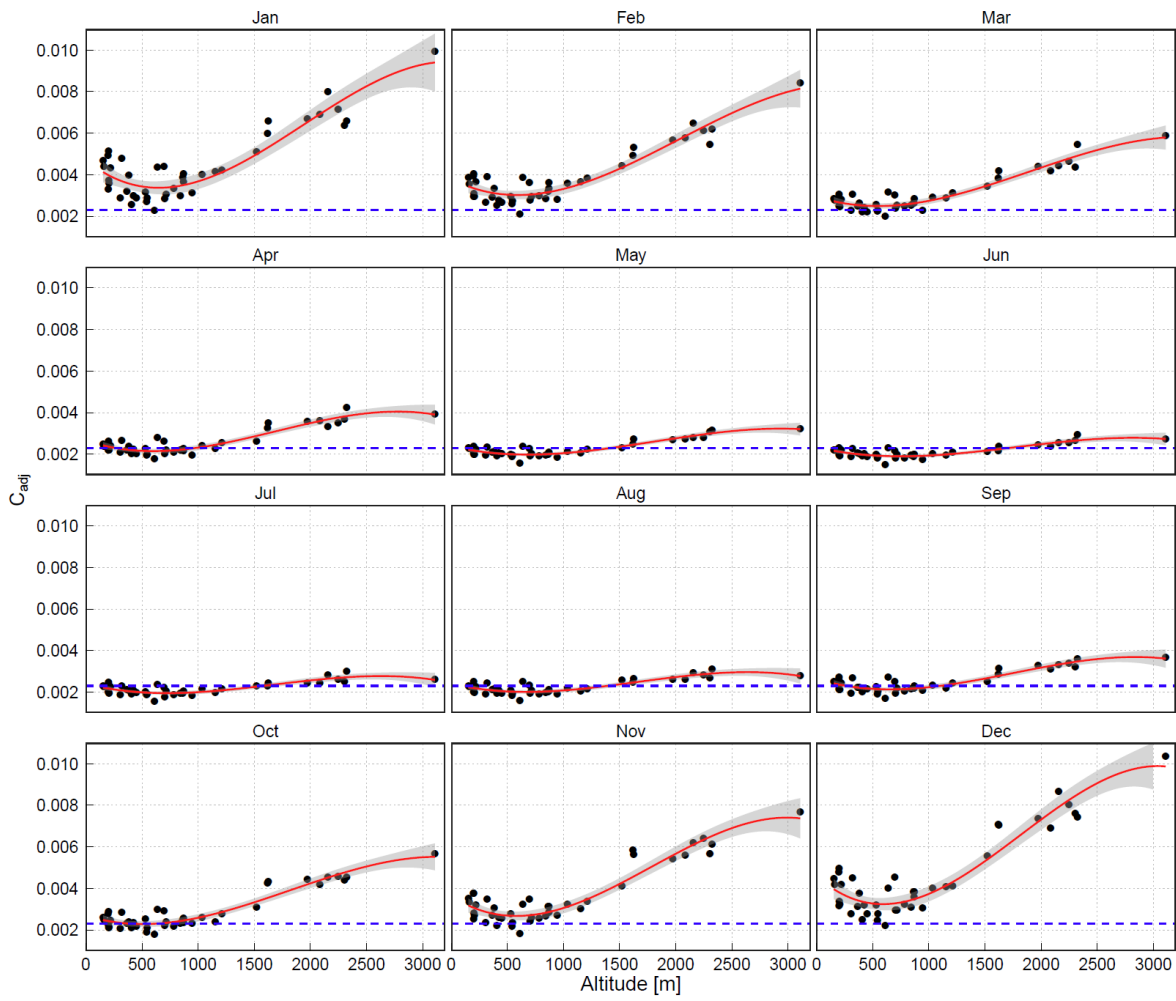


2

3

4 Figure 6. Monthly variations of  $C_{adj}$  with respect to altitude; the black contour line defines the  
5 original Hargreaves Calibration Parameter  $C$  value of 0.0023; stations are binned to classes of  
6 altitude from 100 to 2300 m every 100 m; white areas denote classes of altitude with no  
7 station available.

1

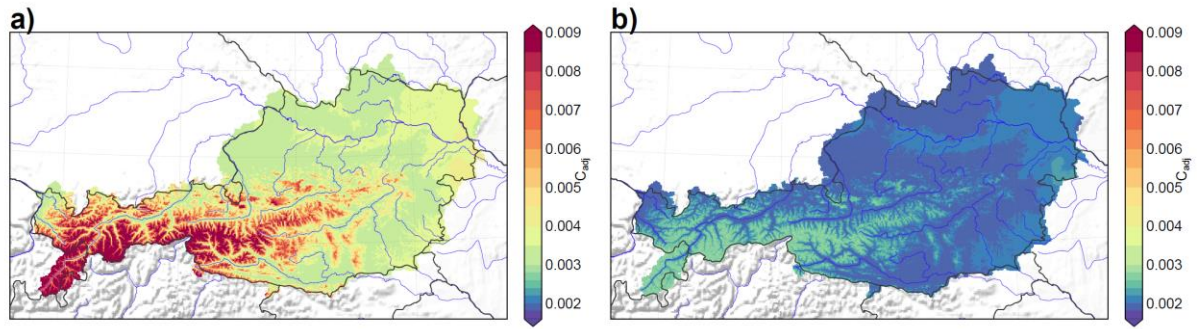


2

3

4 Figure 7. Station-wise monthly third-order polynomial fit of the Hargreaves Calibration  
5 Parameter  $C_{adj}$  against altitude; the blue dotted line indicates the original C value of 0.0023.

1

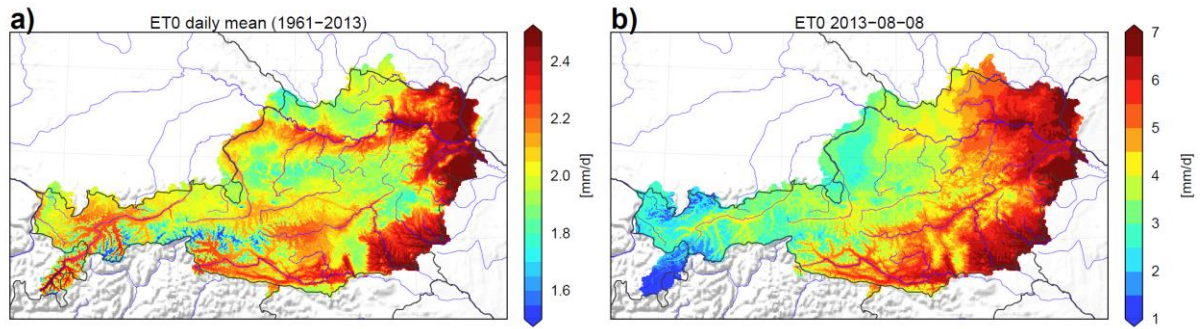


2

3

4 Figure 8. Spatially interpolated  $C_{adj}$  values for January 1<sup>st</sup> (a) and July 1<sup>st</sup> (b).

1



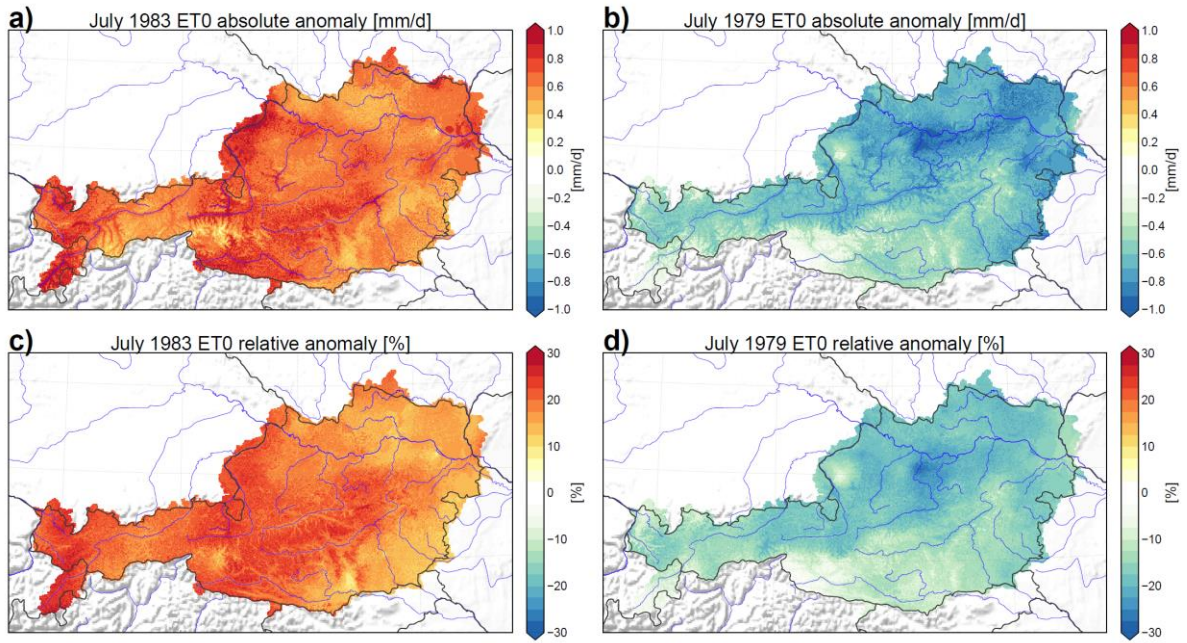
2

3

4 Figure 9. Climatological daily mean ET0 from 1961-2013 (a); example of a daily field of ET0  
5 on August 8<sup>th</sup> 2013 (b).

6

1



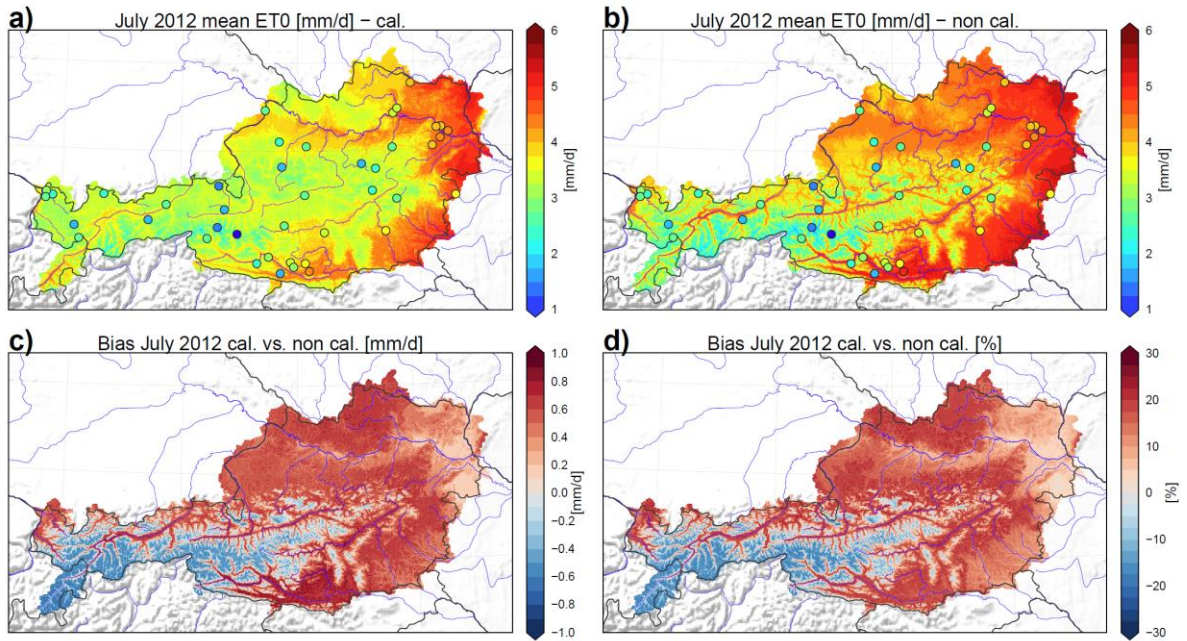
2

3

4 Figure 10. Upper panel: absolute anomalies of ET0 sum in July 1983 (a) and July 1979 (b)  
5 with respect to the climatological mean in July from 1961-2013; lower panel: corresponding  
6 relative anomaly (c, d).

7

1



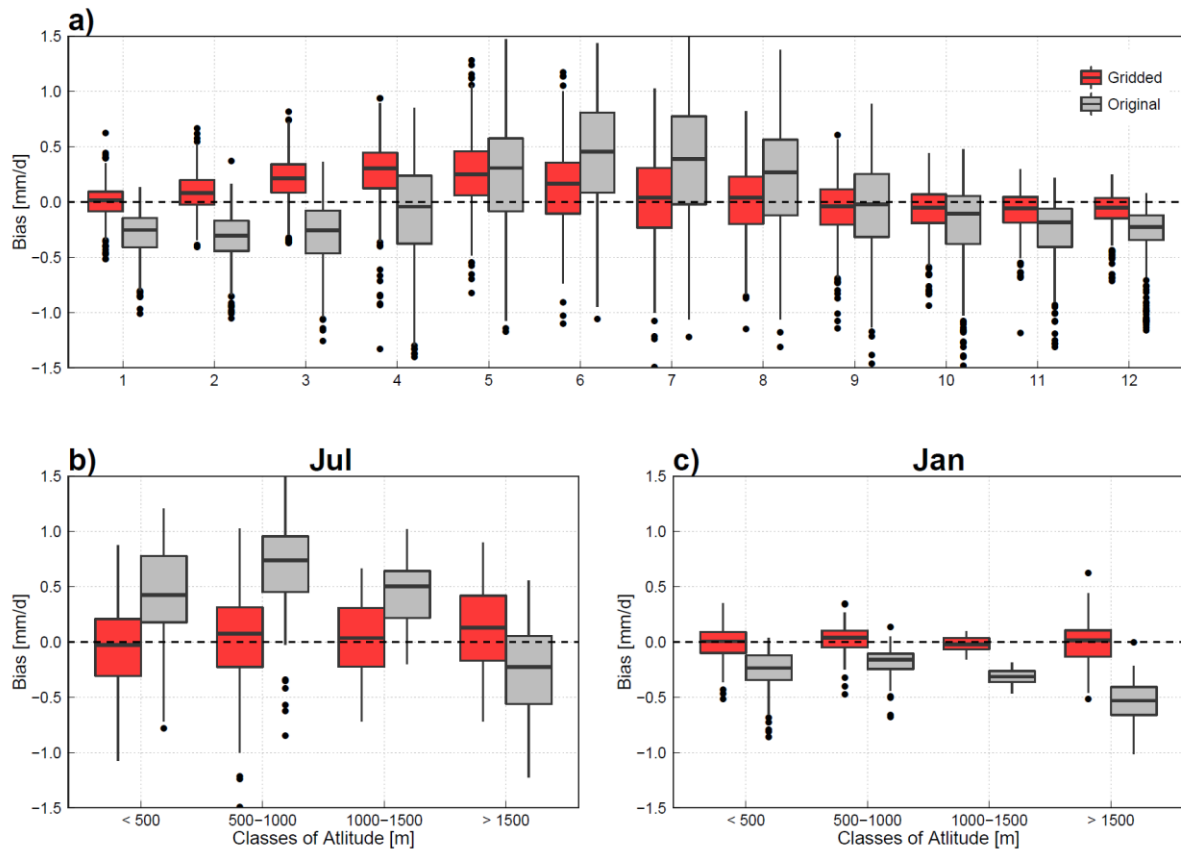
2

3

4 Figure 11. July 2012 monthly mean ET0 based on  $C_{adj}$  values – ET0\_h.c (a), using the  
5 original C of 0.0023 for the whole grid ET0\_h (b) and the corresponding absolute (c) and  
6 relative bias (d); the dots in (a) and (b) denote for the PM ET0 at the stations.

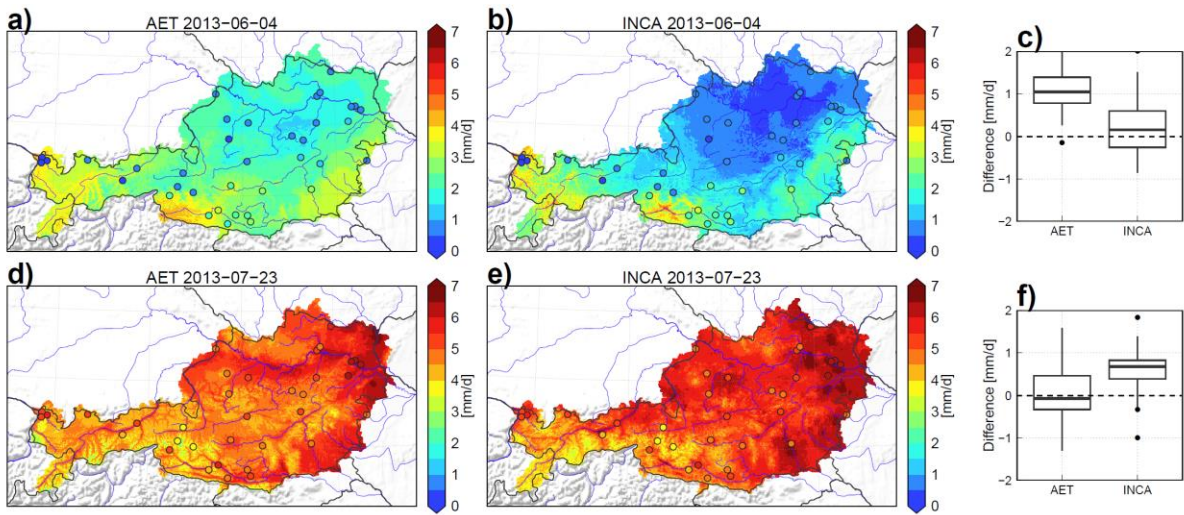
7





1  
2  
3  
4  
5  
6

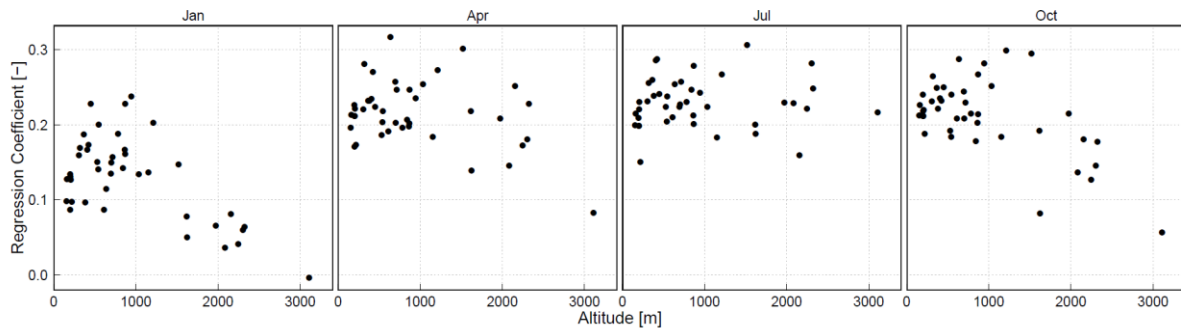
Figure 12. Boxplots of monthly mean bias of the station-wise original Hargreaves ET<sub>0</sub> (grey) and the ARET, re-calibrated ET<sub>0</sub> (red) against Penman-Monteith ET<sub>0</sub> (a); stratified by different classes of altitude in July (b) and January (c).



1  
2  
3  
4  
5  
6  
7

Figure 13. ET0 fields of AET (a, d) and INCA (b, e) and station wise PM ET0 on June 4<sup>th</sup> 2013 (cool and overcast conditions) and July 23<sup>rd</sup> 2013 (warm and mostly sunny conditions) and corresponding differences at grid points closest to a station with PM ET0 of both datasets displayed as boxplots (c, f).

1

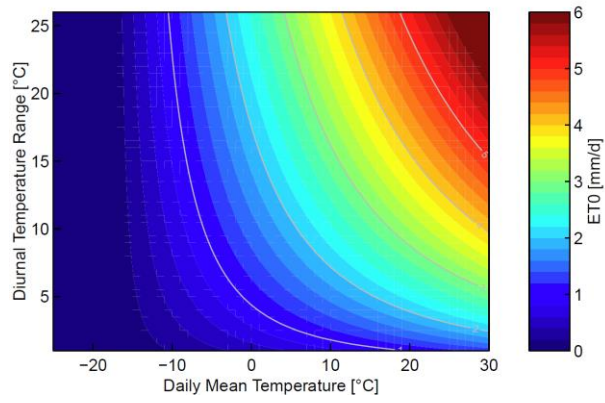


2

3

4 Figure 14. Station-wise linear regression coefficient of the TOA radiation - Global Radiation  
5 ratio against the square root of the Diurnal Temperature Range ( $T_{\max}-T_{\min}$ ) against altitude  
6 represented by black dots in January, April, July and October.

7



1

2

3 Figure 15. ET0 response to varying Daily Mean Temperature and Diurnal Temperature  
4 Range; ET0 values are calculated with 1<sup>st</sup> of April Top of the Atmosphere Radiation and the  
5 original C value of 0.0023.

6

- 1
- 2
- 3
- 4